


# Curvature scaling of the transient convective boundary layer flow along a vertical cylinder: An improved explicit form

Yang Liu <sup>\*</sup>, Yifeng Zhu, and Changhui Liu*School of Ocean Science and Technology, Dalian University of Technology, Dalian 116024, China*

(Received 17 April 2023; accepted 3 August 2023; published 17 August 2023)

In this paper, we use the scaling method to investigate the transient convective boundary layer evolving on the external surface of an isothermally heated vertical cylinder. Our numerical calculations show that a boundary layer flow develops in the vicinity of the heated surface due to the buoyancy effect. We also demonstrate that the thickness and velocity of the boundary layer flow are significantly affected by the curvature effect. Our analysis successfully determines a set of fully explicit scaling laws for the initial and steady flow states over a large parameter range, with Rayleigh numbers ( $Ra$ ) of  $10^7$  to  $10^9$ , Prandtl numbers ( $Pr$ ) of 10 to 100, and aspect ratios ( $A$ ) of 1 to 100. These scaling laws are explicit and easier to use than the previous implicit scaling laws [Phys. Rev. Fluids **7**, 054101 (2022)]. The present scaling laws consist of the flat plate scaling, which accounts for the  $Ra$  and  $Pr$  number dependencies, and a dimensionless explicit curvature coefficient  $\Psi'(A)$ . When the boundary layer is much thinner than the cylinder radius, the proposed scaling laws reduce to the well-known flat boundary layer ones, and the curvature coefficient  $\Psi'(A)$  approaches the unity. When the boundary layer thickness is close to or larger than the cylinder radius, the curvature effect becomes significant, and the curvature coefficient  $\Psi'(A)$  accurately quantifies the curvature effect. Comparison between the scaling laws and numerical calculations shows that most fitting constants  $R^2$  are approximately 0.999, which convincingly validates the proposed scaling laws.

DOI: [10.1103/PhysRevFluids.8.084101](https://doi.org/10.1103/PhysRevFluids.8.084101)

## I. INTRODUCTION

Convective boundary layer flow induced by heating vertical surfaces plays a crucial role in a wide range of domestic and industrial applications, including solar houses, solar chimneys, electronic cooling devices, and radiators. Understanding various aspects of this flow problem is important in fundamental fluid mechanics, encompassing flow behaviors, instability characteristics, and heat transfer properties. Consequently, substantial research efforts have been dedicated to investigating different aspects of convective boundary layer flow over the past few decades [1–9]. Researchers have employed various techniques to study this flow, such as analytical methods [10,11], similarity theory [12–14], linear stability analysis [15–17], direct stability analysis [18–20], direct numerical simulations [21,22], and a range of experimental approaches [23–25]. Among these techniques, the scaling methodology stands out as an exceptionally powerful and promising tool. Pioneered by Patterson and Imberger [26], this approach enables direct estimations, in the form of scaling laws, for key flow variables. Subsequently, the convection and boundary layer research communities recognized the importance of scaling law studies, leading to its gradual adoption across a broader range of flow parameters and its application to various other flow problems.

---

\*yang.liu1@qq.com

In their landmark work, Patterson and Imberger [26] investigated the characteristics of boundary layer flow for fluids with Prandtl numbers  $> 1$ . They successfully derived scales for thickness and velocity that are representative of the boundary layer. However, they did not consider the influence of the Prandtl number in their analysis. Subsequently, Lin *et al.* [27] addressed this issue by analyzing near-wall flow profiles and integrating over three sublayers. They accounted for the effect of the Prandtl number, and this work became a standard approach for subsequent studies involving  $Pr > 1$  fluids. Lin *et al.* [28] extended the scaling method to fluids with Prandtl numbers  $< 1$ . They argued that both the unsteady and viscous terms are equally important during the initial growth state, and their combined effect should balance the driving buoyancy term, thereby enabling scaling for  $Pr < 1$  fluids. The phenomenon of multiscaling behavior in  $Pr < 1$  fluids was also reported, which remains an unresolved topic. In the context of vertically rising buoyant boundary layers encountering horizontal adiabatic surfaces, the formation and propagation of horizontal intrusion flow have been extensively studied, particularly within the cavity research community. Xu *et al.* [29] examined the transient characteristics of intrusion flow, revealing that it consists of either two or four distinct flow regimes, depending on the governing flow parameters. The authors derived corresponding scaling laws for characteristic flow variables and successfully validated them, achieving good agreement with their findings. However, it is important to note that these studies primarily focused on homogeneous conditions without thermal gradients. More recently, researchers such as Liu *et al.* [30–32] and Lin *et al.* [33,34] investigated convective boundary layer flows with thermal gradients. Liu *et al.* [35] argued that, during the initial startup state, the characteristic velocity of the thermal boundary layer is influenced by both the streamwise position and the evolution time, indicating a two-dimensional growth rather than the well-established one-dimensional growth observed in homogeneous problems.

In practical applications, the vertical boundary layer flows can be broadly categorized into two typical scenarios: flow over flat plates and flow over curved surfaces. While a considerable body of literature on flat plate boundary layer flows exists, the availability of scaling laws describing curved boundary layer flows is relatively limited, despite extensive investigations on various aspects of curved boundary layer flows [36–41]. However, in recent years, there has been a growing interest in this area. For instance, Liu *et al.* [42] examined the convective boundary layer flow developing on a horizontal cylinder and derived important scaling laws. They focused on the dependency of various flow variables on the central angle, although the curvature of the horizontal cylinder was assumed to be fixed, and the boundary layer was considered much thinner than the cylinder radius. In a subsequent work, Liu *et al.* [43] further investigated the boundary layer flow over a vertical cylinder and established a set of unified scaling laws that incorporated the effects of curvature, Rayleigh number, and Prandtl number. It was demonstrated that, when the boundary layer is significantly thinner than the cylinder radius, the proposed scaling laws reduce to the well-known flat boundary layer laws proposed by Patterson and Imberger [26] and Lin *et al.* [27]. However, as the cylinder radius or the governing Rayleigh number decreases, the curvature effect becomes increasingly prominent. The proposed scaling laws can accurately describe the transition from flat boundary layers to highly curved ones. It should be noted that some of the proposed scaling laws are expressed implicitly, requiring a careful and challenging implementation process. The scarcity of readily applicable scaling laws motivates this paper.

Our main objective is to improve the previously proposed implicit scaling laws [43] and ultimately obtain a set of unified and explicit scaling laws for curved boundary layer flows. These scaling laws will incorporate the effects of curvature, Rayleigh number, and Prandtl number, allowing for a comprehensive description of the flow behavior. Specifically, we aim to develop scaling laws that exhibit the following characteristics: When the cylinder radius is significantly larger than the boundary layer thickness, the scaling laws should converge to the classical flat-plate scaling laws. However, as the cylinder radius approaches or becomes smaller than the boundary layer thickness, the curvature dependency in the scaling laws should accurately adjust the characteristic flow variables of the boundary layer. It is important to note that the explicit form of these scaling laws will provide a more accessible and practical framework for their implementation. To achieve

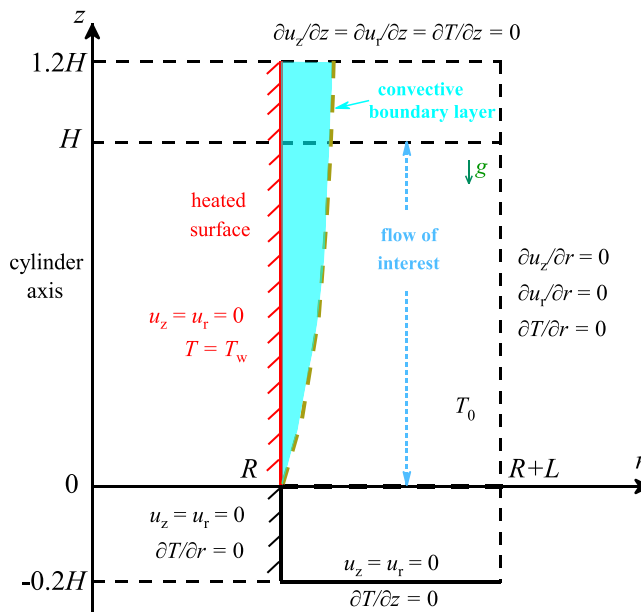


FIG. 1. Schematic of the flow domain.

this goal, this paper is organized as follows. Section II presents a detailed description of the physical problem and the governing mathematical equations. In Sec. III, we conduct scaling analysis. Section IV focuses on examining and highlighting the impact of curvature on the flow variables. Finally, Sec. V provides a summary and conclusions based on the findings of this paper.

## II. THE FLOW AND MATHEMATICAL DESCRIPTIONS

In this paper, we focus on the investigation and analysis of the convective boundary layer flow along the outer surface of a heated vertical cylinder, with specific emphasis on the curvature effect of the cylinder. The schematic representation of the model is illustrated in Fig. 1. Initially, the fluid within the computational domain is at rest and has a uniform temperature of  $T_0$ . At  $t = 0$ , the temperature of the surface of the cylinder is suddenly increased to  $(T_0 + \Delta T)$ , initiating the convective boundary layer flow. In Fig. 1, the vertical axis represents the axis of the cylinder. The computational domain extends to a total height of  $1.4H$ , with  $0.2H$  extensions both upstream and downstream of the region of interest. This configuration is implemented to minimize potential boundary effects, and it is consistent with similar studies conducted in this field [20,44]. The cylinder has a fixed radius of  $R$ , and the width of the computational domain, denoted by  $L$ , is sufficiently large to ensure that the right boundary does not influence the flow. Throughout this paper, the height of the cylinder ( $H$ ) is set to a constant value of 1 m, and the width of the computational domain ( $L$ ) is fixed at 0.24 m. It is worth mentioning that further increasing the value of  $L$  does not affect the results of interest in this paper. It is important to note that, by altering the cylinder radius ( $R$ ), the curvature of the surface of the cylinder is modified. Thus, in this paper, the domain height ( $H$ ) remains fixed, and the curvature effect is realized by varying the cylinder radius ( $R$ ).

The current flow problem is governed by the incompressible continuity equation, Navier-Stokes equations, and the energy conservation equation, with the Boussinesq approximation to account

for the buoyancy term. These equations are formulated in the cylindrical coordinates and can be expressed as follows:

$$\frac{1}{r} \left( u_r + r \frac{\partial u_r}{\partial r} + r \frac{\partial u_z}{\partial z} \right) = 0, \quad (1)$$

$$\frac{\partial u_r}{\partial t} + u_r \frac{\partial u_r}{\partial r} + u_z \frac{\partial u_r}{\partial z} = -\frac{1}{\rho} \frac{\partial p}{\partial r} + \nu \left[ \frac{1}{r} \frac{\partial}{\partial r} \left( r \frac{\partial u_r}{\partial r} \right) + \frac{1}{r} \frac{\partial}{\partial z} \left( r \frac{\partial u_r}{\partial z} \right) \right], \quad (2)$$

$$\frac{\partial u_z}{\partial t} + u_r \frac{\partial u_z}{\partial r} + u_z \frac{\partial u_z}{\partial z} = -\frac{1}{\rho} \frac{\partial p}{\partial z} + \nu \left[ \frac{1}{r} \frac{\partial}{\partial r} \left( r \frac{\partial u_z}{\partial r} \right) + \frac{1}{r} \frac{\partial}{\partial z} \left( r \frac{\partial u_z}{\partial z} \right) \right] + g\beta\Delta T, \quad (3)$$

$$\frac{\partial T}{\partial t} + u_r \frac{\partial T}{\partial r} + u_z \frac{\partial T}{\partial z} = \kappa \left[ \frac{1}{r} \frac{\partial}{\partial r} \left( r \frac{\partial T}{\partial r} \right) + \frac{1}{r} \frac{\partial}{\partial z} \left( r \frac{\partial T}{\partial z} \right) \right], \quad (4)$$

where  $r, z, u_r, u_z, T, \rho, \nu, \kappa, g,$  and  $\beta$  are the radial and vertical coordinates, the two corresponding velocity components, temperature, density, kinematic viscosity, thermal diffusivity, gravitational acceleration, and the thermal expansion coefficient. Here,  $\Delta T$  is the temperature difference characterizing the convection flow, which is calculated by  $\Delta T = T_w - T_0$ . The initial and boundary conditions of the problem are given as follows:

$$\begin{aligned} \frac{\partial u_z}{\partial z} = \frac{\partial u_r}{\partial z} = \frac{\partial T}{\partial z} &= 0 & \text{at } z = 1.2H \\ u_z = u_r = \frac{\partial T}{\partial z} &= 0 & \text{at } z = -0.2H \\ \frac{\partial u_z}{\partial r} = \frac{\partial u_r}{\partial r} = \frac{\partial T}{\partial r} &= 0 & \text{at } r = HA^{-1} + L \\ u_z = u_r &= 0 & \text{at } r = HA^{-1} \text{ and } -0.2H \leq z \leq 1.2H \\ T &= T_w & \text{at } r = HA^{-1} \text{ and } 0 \leq z \leq 1.2H \\ \frac{\partial T}{\partial r} &= 0 & \text{at } r = HA^{-1} \text{ and } -0.2H \leq z < 0 \\ u_z = u_r = 0, T &= T_0 & \text{at all } r \text{ and } z, \text{ at } t < 0, \end{aligned} \quad (5)$$

In this paper, the flow is characterized by three dimensionless parameters: the curvature of the cylinder ( $A$ ), the Rayleigh number ( $Ra$ ), and the Prandtl number ( $Pr$ ), as defined in Eq. (6). It is important to emphasize that the value of  $H$  remains constant throughout this paper, while  $R$  is varied to achieve different surface curvatures. Specifically, a smaller value of  $R$  corresponds to a larger value of  $A$  and a slender cylinder, whereas a larger value of  $R$  corresponds to a smaller value of  $A$  and a thicker cylinder:

$$A = \frac{H}{R}, \quad Ra = \frac{g\beta\Delta TH^3}{\nu\kappa}, \quad Pr = \frac{\nu}{\kappa}. \quad (6)$$

Previous investigators have demonstrated the significant impact of surface curvature on various aspects of the convective boundary layer flow [43,45,46]. Figure 2 provides a schematic representation of the steady-state boundary layer flow at three distinct surface curvatures:  $A = 1, 10,$  and  $100$ . It is evident that the boundary layer thickness becomes increasingly pronounced relative to the cylinder radius when  $R$  is small or  $A$  is large. This observation implies that the curvature effect plays a more prominent role in the boundary layer flow of slender columns. In such cases, the flow exhibits a more pronounced curvature toward the surface than the flow developing along a heated flat plate.

In a previous study [43], implicit scaling laws for the convective boundary layer flow were proposed. However, the implementation procedure for certain physical variables was found to be less straightforward. Therefore, the objective of this paper is to address this issue by providing a set of explicit scaling laws for the flow. To achieve this, it is necessary to first resolve the flow. In this paper, the finite volume method is employed to solve the governing equations. The discretization of the first and second derivative terms in the governing Eqs. (1)–(4) is accomplished using the

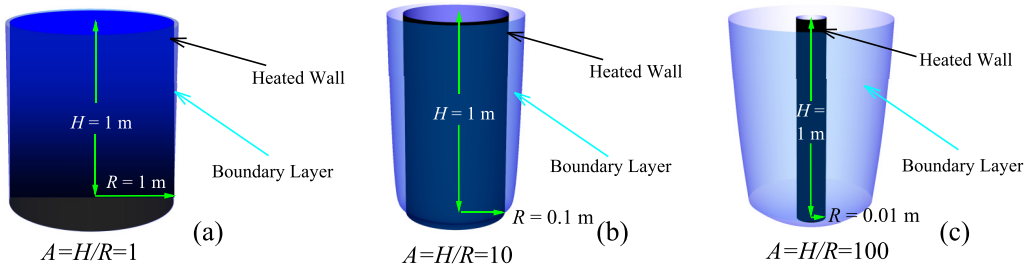


FIG. 2. Schematic of steady-state convective boundary layer at different surface curvatures with the case  $Ra = 1 \times 10^8$  and  $Pr = 40$ : (a)  $A = 1$ , (b)  $A = 10$ , and (c)  $A = 100$ .

second-order central difference scheme. For the unsteady terms, the second-order implicit method is applied. The pressure-velocity coupling method adopts the SIMPLE algorithm. Subsequently, the resulting algebraic equations are solved iteratively using the third-order Runge-Kutta scheme until convergence is attained. In this paper, the scaled residual is utilized as the convergence criterion, with a value of  $10^{-3}$  chosen for both the continuity and Navier-Stokes equations and  $10^{-6}$  for the energy conservation equation. This numerical approach has been widely employed over the past few decades and has proven to be effective and robust for a variety of free convection flow problems [5,6,31].

To ensure that the calculation results are independent of the chosen grid and timestep, grid- and timestep-dependency tests are conducted for the case with  $Ra = 1 \times 10^9$ ,  $Pr = 40$ , and  $A = 10$ . Three computational grids are selected for the grid-dependency test, with varying sizes of the mesh immediately adjacent to the heated surface: 0.3, 0.2, and 0.1 mm, respectively, for the three grids. The inflation factor remains constant at 1.05 in the radial direction. In the streamwise direction, or in the  $z$  direction, the grid adopts an equidistributional mode, and the grid sizes are 0.002, 0.0017, and 0.00083 m for the three meshes. Therefore, the three grids consist of  $500 \times 160$ ,  $600 \times 200$ , and  $1200 \times 320$  cells (in  $H \times L$ ), respectively. Additionally, three timesteps are utilized for the timestep-dependency test. In our previous studies, we demonstrated that extremely high computing cost would be incurred if low- $Ra$  cases use the same timestep as high- $Ra$  cases. To mitigate this issue, the duration of the early state development is utilized as a reference value for determination of the timestep for each specific flow condition. For the case with  $Ra = 1 \times 10^9$ ,  $Pr = 40$ , and  $A = 10$ ,  $\frac{1}{20}$ th,  $\frac{1}{40}$ th, and  $\frac{1}{80}$ th of the early state duration are employed for the timestep-dependency test, which are 60.03, 30.015, and 15.0075 s, respectively. During the numerical calculations, the velocity component in the streamwise direction ( $u_z$ ) is monitored and recorded at a specific location ( $r = 0.11$  m,  $z = 1$  m), which is situated 0.01 m away from the heated surface. The time series of  $u_z$  are plotted in Fig. 3, demonstrating three distinct states of flow development: an initial growth, an oscillatory leading-edge effect (LEE) transition, and a steady state. Figure 3 also demonstrates that the impact of grid resolution and timestep is nearly negligible during the initial and steady states. A detailed analysis of the calculation results reveals that the maximum relative error of the monitored steady-state  $u_z$  is  $\sim 0.28\%$ , indicating that any of the grids and timesteps could be employed for this paper. Therefore, the mesh with  $600 \times 200$  cells and the timestep of  $\frac{1}{40}$ th of the early state duration are adopted for the subsequent calculations. In addition, it is worth mentioning that authors of many previous similar works have suggested that the present mesh could provide satisfactory resolution for the flow parameter ranges, see, e.g., Refs. [26,42].

A comprehensive set of 30 cases is numerically calculated to establish the scaling laws that characterize the curved boundary layer flow. The specific parameters for each calculated case are presented in Table I. It is important to note that the Rayleigh number under investigation is no higher than  $10^9$ , and this will lead to the laminar flow regime with no fluctuations in flow parameters. Previous numerical studies demonstrated that, for  $Pr > 1$  flat-plate boundary layer flows, the critical

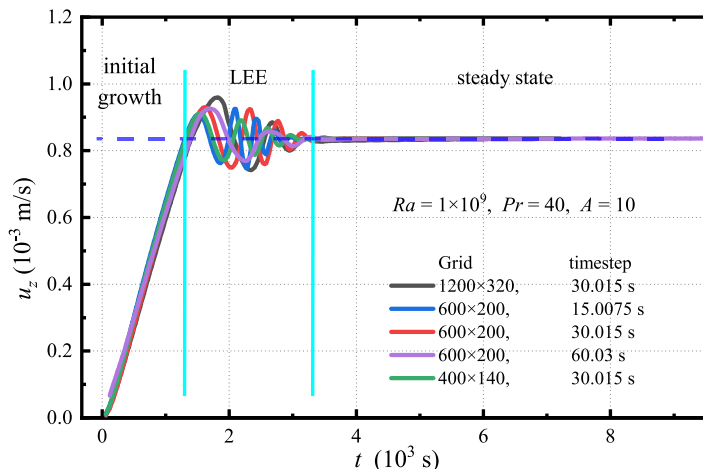


FIG. 3. Grid and time step dependency tests with the case  $Ra = 1 \times 10^9$ ,  $Pr = 40$ , and  $A = 10$ , monitored at ( $r = 0.11$  m,  $z = 1$  m).

Rayleigh number for turbulent transition is generally  $> 10^{10}$  (between  $10^{10}$  and  $10^{11}$ ), which is at least one order of magnitude higher than the largest  $Ra$  adopted in this paper. Additionally, numerous previous similar studies confirmed that no bifurcations are numerically observed for  $10^6 \leq Ra \leq 10^9$  [26,42]. This ensures all the flow conditions examined in this paper are laminar.

### III. SCALING ANALYSIS

In a previous study [43], implicit scaling laws were proposed to describe the curved boundary layer studied in this paper. The derivation of these scaling laws suggests that they can be expressed in a general form, as shown in Eq. (7). In this equation,  $\omega$  represents a flow variable, such as the characteristic velocity or thickness. The function  $h(r, z, t)$  corresponds to the scaling law associated with a flat-plate flow for the variable  $\omega$ . Additionally,  $\Psi(\omega, R)$  is a dimensionless coefficient that accounts for the curvature effect. The determination of the function  $\Psi(\omega, R)$  was achieved through a standard data fitting procedure, involving numerical regression to obtain the unknown curvature coefficients. Equation (7) describes how  $\omega$  is affected by other flow variables, and the scaling law is in the implicit form if the curvature dependency  $\Psi$  includes the effect of  $\omega$ . Conversely, the scaling law is in the explicit form if  $\omega$  is not included in the function  $\Psi$ . In this paper, the curvature dependency in implicit and explicit scaling laws is respectively denoted by  $\Psi$  and  $\Psi'$ . Authors of the previous study discovered that the scaling laws for the boundary layer thickness are implicit,

TABLE I. Flow parameters of the calculated case run.

Case No.	$Ra$	$Pr$	$A$
1–7	$1 \times 10^7$	40	1, 2, 5, 10, 20, 50, 100
8–14	$1 \times 10^8$	10	1, 2, 5, 10, 20, 50, 100
15–21	$1 \times 10^8$	40	1, 2, 5, 10, 20, 50, 100
22–28	$1 \times 10^8$	70	1, 2, 5, 10, 20, 50, 100
29	$1 \times 10^8$	100	10
30	$1 \times 10^9$	40	10

while the scales for the characteristic velocity are explicit [43]:

$$\omega \sim h(r, z, t)\Psi(\omega, R). \quad (7)$$

In this paper, our objective is to propose a comprehensive set of fully explicit scaling laws by replacing the function  $\Psi(\omega, R)$  with  $\Psi'(R)$ . To accomplish this, numerical regression is conducted using the cases listed in Table I to accurately determine the dependency on  $R$ . It is worth noting that this scaling methodology is widely employed in the convection and boundary layer research communities and has been extensively utilized over the past several decades [47–49]. In this paper, both the initial growth and steady states are analyzed, and a range of scaling laws that quantify these two states are determined.

At  $t = 0$ , the temperature of the cylinder surface experiences a sudden increase by  $\Delta T$ , which serves as the triggering mechanism for the current boundary layer flow. Patterson and Imberger [26] proposed that this physical process can be described by a balance between the unsteady term and the radial conduction term in the temperature conservation equation, i.e., Eq. (4), which can be expressed as follows:

$$\frac{\partial T}{\partial t} \sim \kappa \frac{1}{r} \frac{\partial}{\partial r} \left( r \frac{\partial T}{\partial r} \right). \quad (8)$$

In the previous study [43], the following implicit scaling law for the boundary layer thickness during the initial growth state was obtained:

$$\Delta_t \sim \kappa^{1/2} t^{1/2} \left( \frac{R + 0.3\Delta_t}{R + 0.5\Delta_t} \right)^{1/2}. \quad (9)$$

It is widely recognized that  $\kappa^{1/2} t^{1/2}$  represents the scaling for the boundary layer thickness on a flat plate during the initial growth state. The term  $\Psi(\Delta_t, R) = [(R + 0.3\Delta_t)/(R + 0.5\Delta_t)]^{1/2}$  accounts for the curvature effect. One needs to determine the root of Eq. (9) to obtain the early state boundary layer thickness, making it challenging to use this implicit form. Therefore, it is crucial to eliminate  $\Delta_t$  from the right-hand side of Eq. (9) to derive an alternative explicit scaling law. Considering previous findings, we propose the following form for  $\Psi'(R)$ :

$$\Psi'(R) = \frac{\prod_{i=1}^n R_m^{j(i)}}{\prod_{i=1}^n R_n^{j(i)}}, \quad (10)$$

in which  $R_m$  and  $R_n$  are separately defined in Eqs. (11) and (12), and  $m$  and  $n$  are coefficients to be determined:

$$R_m = R + mH = R(1 + mA), \quad (11)$$

$$R_n = R + nH = R(1 + nA). \quad (12)$$

In physics, it is evident that, when the radius of the cylinder is significantly large, the curved boundary layer flow closely resembles the flat-plate problem. Conversely, when the radius is much smaller than the boundary layer thickness, the curvature effect becomes dominant. This means that, in Eqs. (11) and (12), as  $A$  approaches zero (i.e.,  $R \rightarrow \infty$ ), the present curved boundary layer flow reduces to the classical flat-plate problem, where  $R_m/R_n = 1$  and  $\Psi'(R) = 1$ . In this special scenario, the thermal boundary layer thickness becomes  $\Delta_t \sim \kappa^{1/2} t^{1/2}$ , which agrees with many previous flat-plate works [26,50,51]. Similarly, authors of the previous study [43] demonstrated the effectiveness of the regression technique when  $A$  is very large. Therefore, this regression approach is inherited in this paper. It is important to clarify that  $\Psi'(R)$  in Eq. (10) will be expressed as  $\Psi'(A)$  for the rest of this paper, as the cylinder radius  $R$  can be eliminated, as shown in Eqs. (11) and (12).



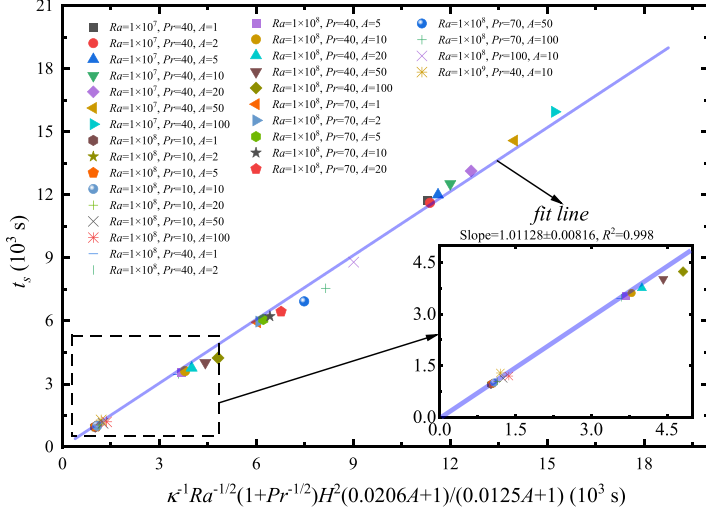


FIG. 4. Numerically obtained  $t_s$  vs its scaling law  $\kappa^{-1} Ra^{-1/2} (1 + Pr^{-1/2}) H^2 (0.0206A + 1) / (0.0125A + 1)$ .

Authors of previous scaling studies for natural convection boundary layer flows have suggested that the boundary layer thickness in the initial development state could be calculated by

$$\Delta_t \sim \frac{\Delta_{t_s}}{t_s^{1/2}} t^{1/2}. \quad (13)$$

The present  $\Delta_t$  can also be described with the equation mentioned above. It is evident in Eq. (13) that  $\Delta_t$  is determined by both  $\Delta_{t_s}$  and  $t_s$ . Based on our previous discussion, both  $\Delta_{t_s}$  and  $t_s$  can be rewritten in the form of Eq. (7), where each of them involves two unknown coefficients, represented by  $m$  and  $n$ . Considering these factors, the estimation for the present  $\Delta_t$  is hereby given by the following equation:

$$\Delta_t \sim \kappa^{1/2} t^{1/2} \frac{(1 + n_{t_s} A)^{1/2}}{(1 + m_{t_s} A)^{1/2}} \frac{(1 + m_{dt_s} A)}{(1 + n_{dt_s} A)}, \quad (14)$$

where  $m_{t_s}$  and  $n_{t_s}$  are the coefficients for  $t_s$ , and  $m_{dt_s}$  and  $n_{dt_s}$  are the coefficients for steady-state thermal boundary layer thickness, respectively. It is important to note that  $t_s$  refers to the duration of the initial growth of thermal boundary layer thickness. The term  $(1 + n_{t_s} A)^{1/2} (1 + m_{dt_s} A) / (1 + m_{t_s} A)^{1/2} (1 + n_{dt_s} A)$  corresponds to  $\Psi'_1(A)$ , which represents the coefficient reflecting the curvature effect on the early state boundary layer thickness. It is worth noting that, because the scaling relation of  $\Delta_t$  is calculated by Eq. (13), the curvature dependency becomes a bit complicated in comparison with the steady-state law.

The cutoff time for the initial growth state includes both a flat-plate term  $t_s$  and a curvature coefficient  $\Psi_2(\Delta_{t_s}, A)$  [43], as described in Eq. (15). It is worth noting that this equation is also implicit since the steady-state boundary layer thickness, i.e.,  $\Delta_{t_s}$ , is directly related to  $t_s$ . In this paper, we propose an alternative estimation of the curvature effect using  $\Psi'_2(A) = (1 + m_{t_s} A) / (1 + n_{t_s} A)$ . Consequently, we can come to Eq. (16) as follows:

$$t_s \sim \frac{H^2 (1 + Pr^{-1/2})}{\kappa Ra^{1/2}} \Psi_2(\Delta_{t_s}, A), \quad (15)$$

$$t_s \sim \frac{H^2 (1 + Pr^{-1/2})}{\kappa Ra^{1/2}} \frac{(1 + m_{t_s} A)}{(1 + n_{t_s} A)}. \quad (16)$$



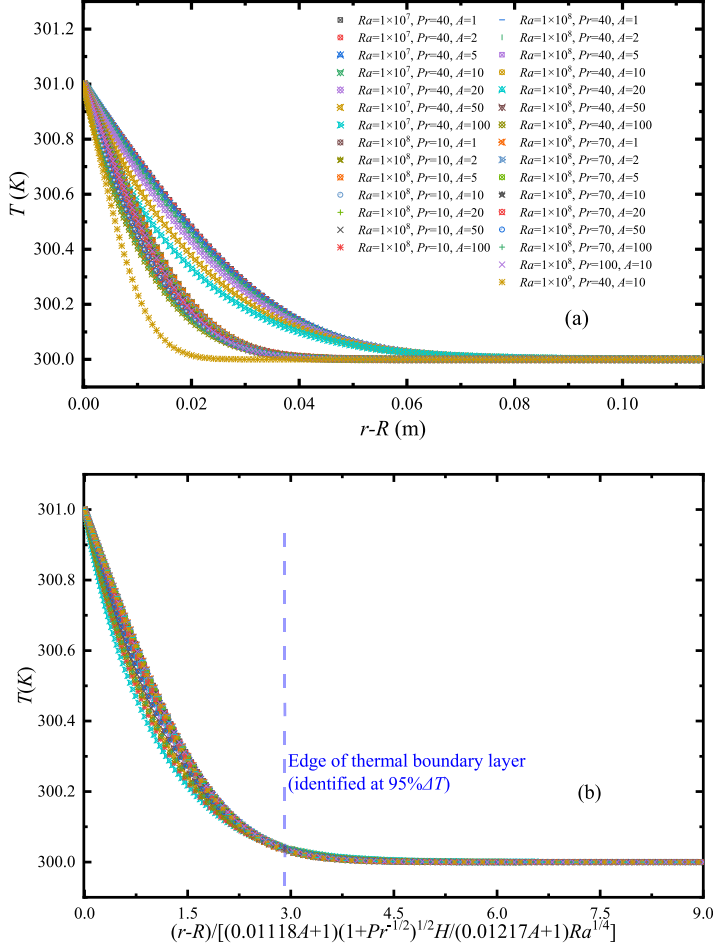


FIG. 5. Temperature profiles in the vicinity of the heated surface in the steady state (measured at  $z = 1$ ): (a) raw data and (b) normalized profiles.

To determine the coefficients  $m_{t_s}$  and  $n_{t_s}$ , a series of numerical cases are calculated, and the corresponding results are numerically regressed and compared with the proposed Eq. (16). In this regard, a wide range of flow parameters are considered and utilized for the simulations, including  $Pr = 10, 40, 70$ , and  $100$ ;  $Ra = 10^7, 10^8$ , and  $10^9$ ; and  $A = 1, 2, 5, 10, 20, 50$ , and  $100$ . During the calculations, the time instance at which the thermal boundary layer thickness first reaches its steady-state value is taken as  $t_{s_s}$ , and all data are monitored at  $z = 1$ . The results of the numerical regression process are presented in Fig. 4. This figure indicates that the combination of  $m_{t_s} = 0.0206$  and  $n_{t_s} = 0.0125$  adequately characterizes the flow, with a fitting constant  $R^2$  of 0.998. Consequently, Eq. (16) can be expressed in the following explicit form:

$$t_s \sim \frac{H^2(1 + Pr^{-1/2})(1 + 0.0206A)}{\kappa Ra^{1/2}(1 + 0.0125A)}. \quad (17)$$

The above scaling law could also be recast by Eq. (18), considering that the slope has been accurately determined in Fig. 4:

$$t_s = 1.01128 \frac{H^2(1 + Pr^{-1/2})(1 + 0.0206A)}{\kappa Ra^{1/2}(1 + 0.0125A)}. \quad (18)$$

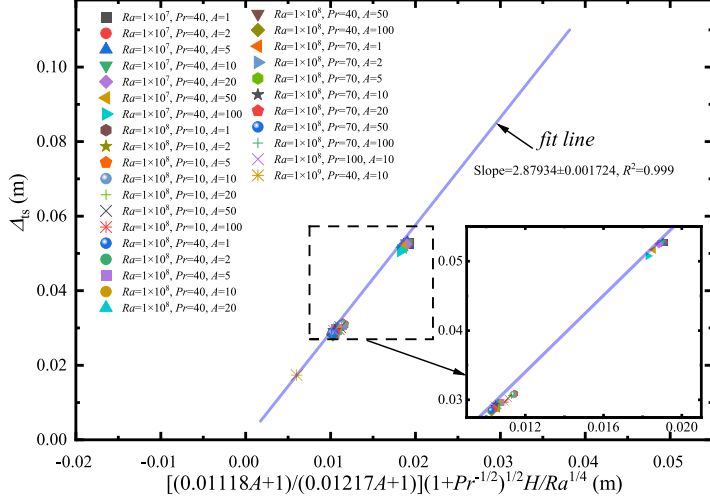


FIG. 6. Numerically obtained steady-state boundary layer thickness  $\Delta_{ts}$  compared against its scaling law  $[(0.01118A + 1)/(0.01217A + 1)](1 + \text{Pr}^{-1/2})^{1/2} H/Ra^{1/4}$ .

According to Eq. (13), we need to obtain the scaling law of  $\Delta_{ts}$  before  $\Delta_t$  could be eventually described. Similar to the above discussions,  $\Delta_{ts}$  was estimated by an implicit scaling  $\Delta_{ts} \sim H\text{Ra}^{-1/4}(\text{Pr}^{-1/2} + 1)^{1/2} \Psi_3(\Delta_{ts}, A)$  in Ref. [43] and an explicit form  $\Delta_{ts} \sim H\text{Ra}^{-1/4}(\text{Pr}^{-1/2} + 1)^{1/2} \Psi'_3(A)$  is assumed in this paper. The function  $\Psi'_3(A)$  is in the form of  $(1 + m_{dts}A)/(1 + n_{dts}A)$ , where the coefficients  $m_{dts}$  and  $n_{dts}$  are also to be determined from numerical regression. Figure 5(a) depicts the raw data of temperature profiles adjacent to the heated surface under various flow conditions at  $z = 1$ . It is seen that the steady-state boundary layer thickness does depend on the various flow parameters. Figure 5(b) demonstrates that all the curves collapse together when the horizontal coordinate is normalized by the  $\Delta_{ts}$  scaling with  $m_{dts} = 0.01118$  and  $n_{dts} = 0.01217$ . This suggests that Eq. (19) reasonably quantifies  $\Delta_{ts}$ . It is worth noting that, similar to the procedure for determining  $m_{ts}$  and  $n_{ts}$ , the same set of cases is used to determine  $m_{dts}$  and  $n_{dts}$ :

$$\Delta_{ts} \sim H\text{Ra}^{-1/4}(\text{Pr}^{-1/2} + 1)^{1/2} \left( \frac{0.01118A + 1}{0.01217A + 1} \right). \quad (19)$$

To further validate the proposed scaling law in Eq. (19), a direct comparison is made between the numerically obtained  $\Delta_{ts}$  and the proposed scaling law in Fig. 6. The figure shows that a straight line approximately passes through all the data points with a fitting constant  $R^2 = 0.999$ . This further confirms the accuracy of the scaling law proposed in Eq. (19). It is important to note that the edge of the thermal boundary layer is identified at the position where the local temperature drops to  $(T_w - 95\% \Delta T)$ . Interestingly, Fig. 6 reveals three distinct clusters of data points, and they in fact correspond to the three different Rayleigh numbers considered. However, within each Rayleigh number, the data points do not significantly scatter. This indicates that  $\Delta_{ts}$  is more sensitive to the Rayleigh number than the curvature effect ( $A$ ) and Prandtl number ( $\text{Pr}$ ). The present data also demonstrate that the curvature dependency in Eq. (19) is 0.999 at  $A = 1$  and 0.955 at  $A = 100$ . This suggests the steady-state boundary layer thickness does not profoundly change with  $A$ , and this is consistent with our simulations. The fitting constant  $R^2 = 0.999$  in Fig. 6 suggests that the present curvature dependency in Eq. (19) could well capture the curvature effect.

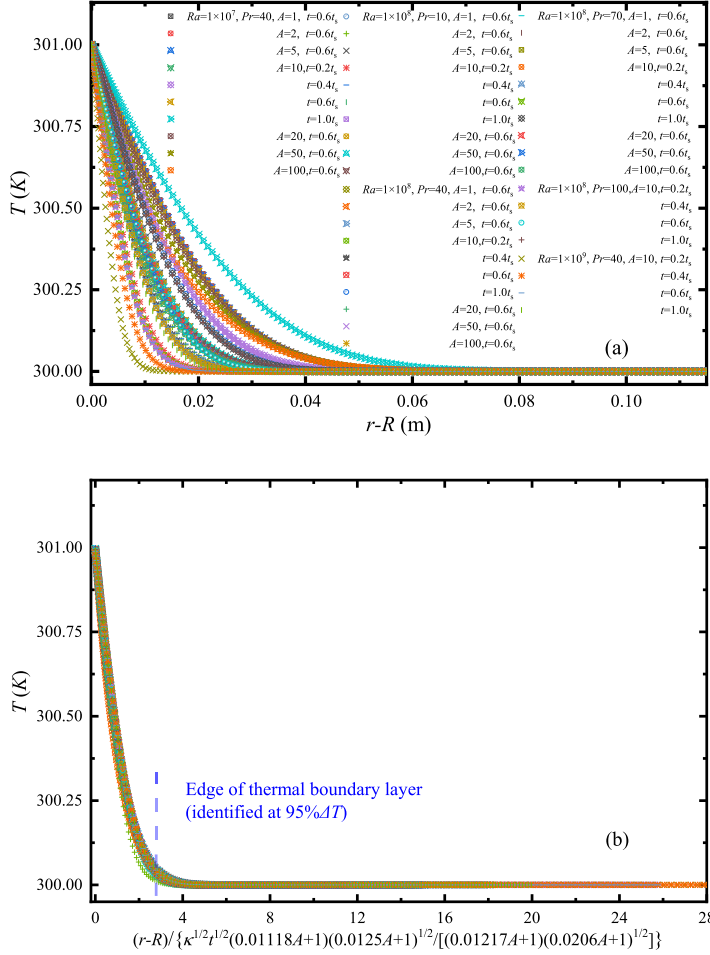


FIG. 7. Temperature profiles in the vicinity of the heated surface in the initial growth state (measured at  $z = 1$  and recorded at  $t = 0.1t_s, 0.2t_s, 0.4t_s, 0.6t_s$ , and  $1.0t_s$ ): (a) raw data and (b) normalized profiles.

By incorporating the slope determined in Fig. 6, Eq. (19) could be rearranged into the following exact form:

$$\Delta_{ts} = 2.87934HRa^{-1/4}(Pr^{-1/2} + 1)^{1/2} \left( \frac{0.01118A + 1}{0.01217A + 1} \right). \quad (20)$$

Therefore, by substituting Eqs. (17) and (19) into Eq. (13), we can derive the scaling law for the early state boundary layer thickness as follows:

$$\Delta_t \sim \kappa^{1/2} t^{1/2} \frac{(1 + 0.0125A)^{1/2} (1 + 0.01118A)}{(1 + 0.0206A)^{1/2} (1 + 0.01217A)}. \quad (21)$$

Temperature profiles adjacent to the heated cylindrical surface are plotted in Fig. 7(a) for the early state at various flow parameters, using the radial coordinate ( $r-R$ ). The curves exhibit some scattering, indicating that the boundary layer thickness is influenced by the corresponding parameters. However, it can be observed in Fig. 7(b) that all the profiles approximately converge onto the same curve when the radial coordinate ( $r-R$ ) is normalized by Eq. (21). This indicates that Eq. (21) accurately captures the boundary layer thickness for the initial growth state.

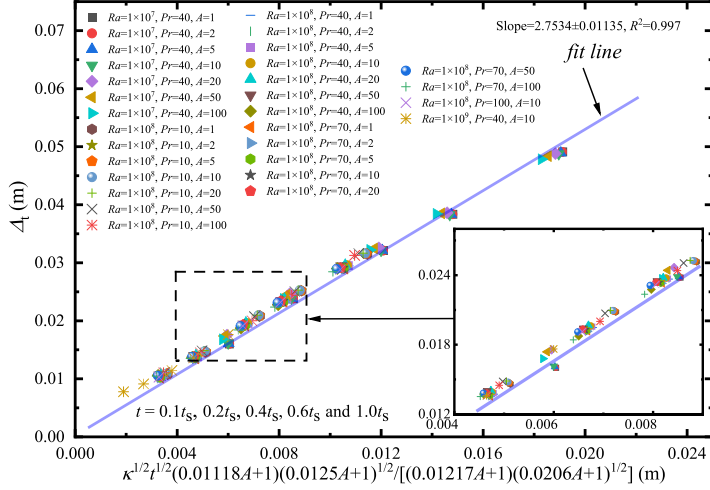


FIG. 8. Numerically obtained early state boundary layer thickness  $\Delta_t$ , compared with its scaling law.

The numerically determined early state boundary layer thicknesses at different  $Ra$ ,  $Pr$ , and  $A$  values are summarized and plotted against the scaling law of  $\Delta_t$  at five time instants in Fig. 8. All data points align closely along a straight line, with a fitting constant  $R^2$  of 0.997, thereby confirming the validity of the proposed scaling law given in Eq. (21). It is important to note that, unlike the results for steady-state thickness shown in Fig. 6, the data points in Fig. 8 scatter. This suggests that the early state  $\Delta_t$  is also sensitive to  $Pr$  and  $A$ .

Figure 9(a) depicts the temporal growth of the boundary layer thickness at various flow conditions. It is important to note that the steady-state boundary layer thickness falls at approximately three distinct values, corresponding to the three Rayleigh numbers considered in this paper. This observation is consistent with our previous analyses, as seen in Fig. 6 and Eq. (19). In Fig. 9(b), the ordinate is normalized by the scaling of  $\Delta_{t_s}$ , while the abscissa is made dimensionless by  $(t/t_s)^{1/2}$ . This figure indicates that, by employing such normalization, all the data points almost collapse onto the same curve, except for the flow behaviors affected by the LEE. Furthermore, it demonstrates that the boundary layer thickness grows linearly with  $\sim t^{1/2}$  during the initial growth state, which agrees with the scaling law given by Eq. (21). Additionally, it is evident that the normalized steady-state boundary layer thickness approaches a consistent value, further validating the appropriateness of Eq. (19).

By incorporating the slope determined in Fig. 9(b), Eq. (21) can be recast as follows:

$$\Delta_t = 2.7534 \kappa^{1/2} t^{1/2} \frac{(1 + 0.0125A)^{1/2} (1 + 0.01118A)}{(1 + 0.0206A)^{1/2} (1 + 0.01217A)}. \quad (22)$$

Lin *et al.* [52] suggested that, in certain convective flows, the cutoff time for the early state growth of the thermal boundary layer may differ from that of the viscous layer. Consistent with their findings, we have also found that significant deviations in the  $Ra$  dependency arise when using Eq. (17), which represents the cutoff time for the thermal boundary layer, to describe the development of the viscous layer in this paper. To tackle this problem, Lin *et al.* [52] proposed a method that involves separately regressing and determining the two cutoff times. We chose to follow this approach in this paper. Similar to the method used to determine  $\Delta_t$ , i.e., Eq. (13), the characteristic velocity of the boundary layer  $u_{mz}$  can be correlated with its steady-state value  $u_{mzs}$ , using the following scaling relation, where  $t_{sv}$  represents the cutoff time for the initial growth of the

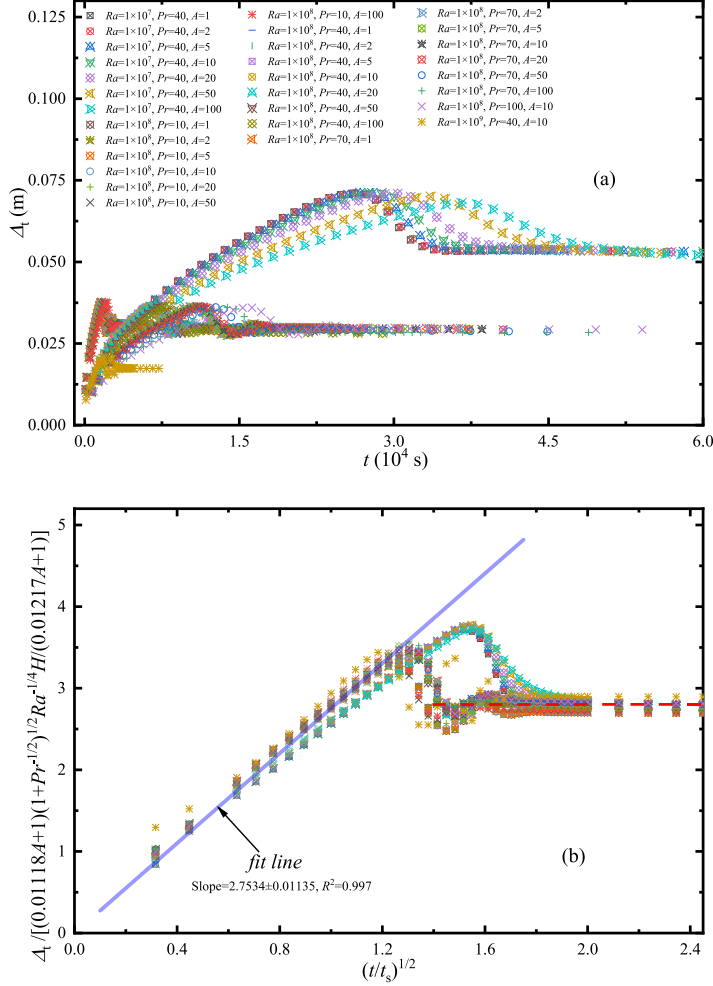


FIG. 9. Temporal growth of boundary layer thickness: (a) raw data and (b) normalized results.

viscous layer:

$$u_{mz} \sim \frac{u_{mzs}}{t_{sv}} t. \quad (23)$$

Equation (23) indicates that, to determine  $u_{mz}$ , we need to obtain the scaling laws for  $t_{sv}$  and  $u_{mzs}$  first. We assume that  $t_{sv}$  follows the following form, where  $\Psi'_4(A)$  represents the curvature effect, and an exponent  $\alpha$  is assumed for the Rayleigh number dependency:

$$t_{sv} \sim \frac{H^2(1 + Pr^{-1/2})}{\kappa Ra^\alpha} \Psi'_4(A) \sim \frac{H^2(1 + Pr^{-1/2})}{\kappa Ra^\alpha} \frac{(1 + m_{t_{sv}}A)}{(1 + n_{t_{sv}}A)}. \quad (24)$$

Numerical calculations are carried out to determine the coefficients  $m_{t_{sv}}$ ,  $n_{t_{sv}}$ , and  $\alpha$ , covering a wide range of flow parameters, i.e., at  $Pr = 10, 40, 70,$  and  $100$ ;  $Ra = 10^7, 10^8,$  and  $10^9$ ; and  $A = 1, 2, 5, 10, 20, 50,$  and  $100$ . The value of  $t_{sv}$  is obtained when the instantaneous velocity  $u_z$  first reaches its steady-state value, with the monitoring location set at  $z = 1$ . Based on the results shown in Fig. 10, it is found that the combination of  $m_{t_{sv}} = 0.0206$ ,  $n_{t_{sv}} = 0.0125$ , and  $\alpha = 0.659$  can accurately describe the temporal development of the viscous layer, with a fitting constant  $R^2$  of

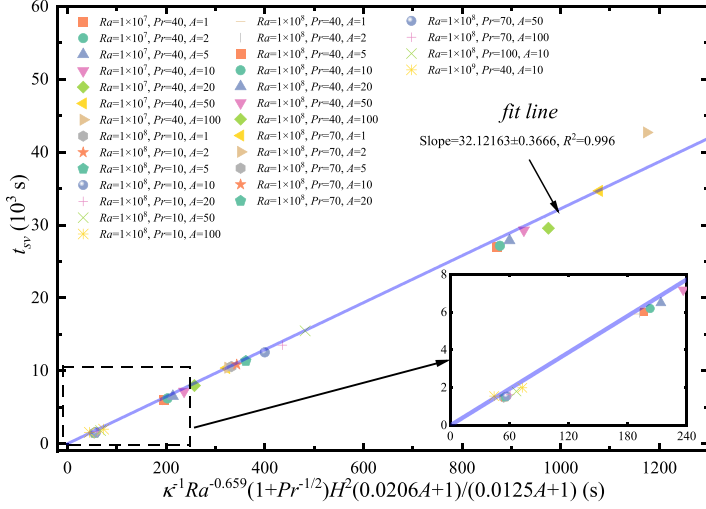


FIG. 10. Numerically obtained  $t_{sv}$  compared against the scaling law  $\kappa^{-1}Ra^{-0.659}(1 + Pr^{-1/2})H^2(0.0206A + 1)/(0.0125A + 1)$ .

0.996. Therefore, we can come to the scaling law for  $t_{sv}$  as follows:

$$t_{sv} \sim \frac{H^2(1 + Pr^{-1/2})(1 + 0.0206A)}{\kappa Ra^{0.659}(1 + 0.0125A)}. \quad (25)$$

Based on the results presented in Fig. 10, it is known that the numerically determined  $t_{sv}$  values are approximately 32.12163 times larger than the scaling values. Considering this, we can rearrange Eq. (25) in the following exact form:

$$t_{sv} = 32.12163 \frac{H^2(1 + Pr^{-1/2})(1 + 0.0206A)}{\kappa Ra^{0.659}(1 + 0.0125A)}. \quad (26)$$

Authors of previous studies have suggested that the characteristic velocity of flat-plate problems is described by  $\kappa Ra^{1/2} H^{-1} (1 + Pr^{-1/2})^{-1}$  [27]. In this paper, the curvature effect on  $u_{mzs}$  is accounted for by  $\Psi'_5(A)$ , which is also in the form of  $(1 + m_{uzs}A)/(1 + n_{uzs}A)$ . Our numerical regression suggests that, when  $m_{uzs} = 0.0249$  and  $n_{uzs} = 0.0338$ , the calculated results could be best matched. This process is shown in Fig. 11, where all data converge onto the same straight line, and the regression constant  $R^2$  equals 0.999. Hence, it leads to the scaling relation in Eq. (27). Note that the maximum velocity component in the  $z$  direction, i.e., the maximum  $u_z$ , is taken as the numerically determined characteristic velocity:

$$u_{mzs} \sim \kappa Ra^{1/2} H^{-1} (1 + Pr^{-1/2})^{-1} \left( \frac{0.0249A + 1}{0.0338A + 1} \right). \quad (27)$$

To determine the scaling of  $\Delta_{vis}$  for the present curved boundary layer, we assume that  $\Delta_{vis}$  follows the scaling law  $\Delta_{vis} \sim (1 + Pr^{-1/2})^{-1/2} H Ra^{-1/4} \Psi'_6(A)$ , where  $\Psi'_6(A)$  takes the form of  $(1 + m_{dvs}A)/(1 + n_{dvs}A)$ . The coefficients  $m_{dvs}$  and  $n_{dvs}$  can be obtained through a numerical fitting process using the prescribed cases mentioned earlier. It is noted that the velocity component  $u_z$  maximizes at  $r = R + \Delta_{vis}$  in the  $r$  direction.

Figure 12 shows that the numerical results agree well with the scaling law when the values of  $m_{dvs}$  and  $n_{dvs}$  are 0.02479 and 0.03737, respectively. This leads to the following scaling law for

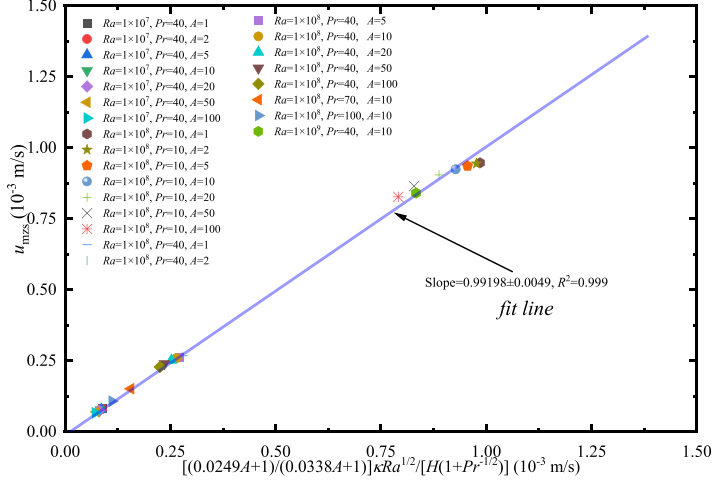


FIG. 11. Numerically obtained steady-state characteristic velocity  $u_{mzs}$  compared against its scaling law  $[(0.0249A + 1)/(0.0338A + 1)]\kappa Ra^{1/2}/[H(1 + Pr^{1/2})]$ .

$\Delta_{vis}$ :

$$\Delta_{vis} \sim HRa^{-1/4}(1 + Pr^{-1/2})^{-1/2} \left( \frac{0.02479A + 1}{0.03737A + 1} \right). \quad (28)$$

This scaling relation can be rearranged by incorporating the determined slope from Fig. 12 as follows:

$$\Delta_{vis} = 1.99085HRa^{-1/4}(1 + Pr^{-1/2})^{-1/2} \left( \frac{0.02479A + 1}{0.03737A + 1} \right). \quad (29)$$

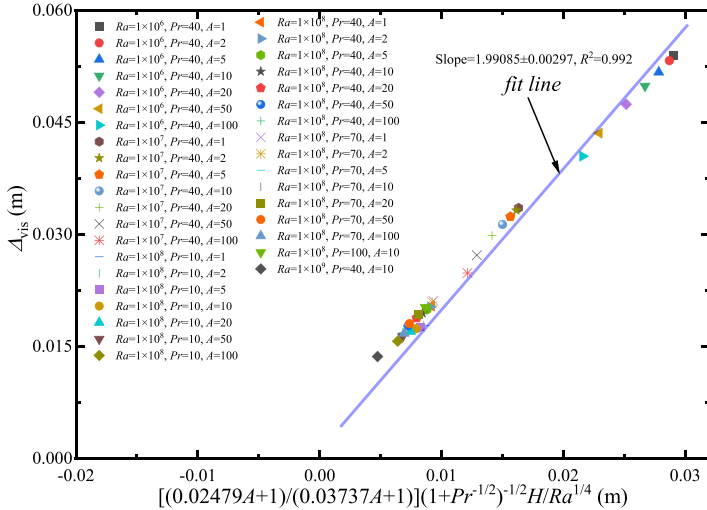


FIG. 12. Numerically obtained steady-state inner viscous layer thickness  $\Delta_{vis}$  against its scaling law  $[(0.02479A + 1)/(0.03737A + 1)](1 + Pr^{-1/2})^{-1/2}HRa^{-1/4}$ .



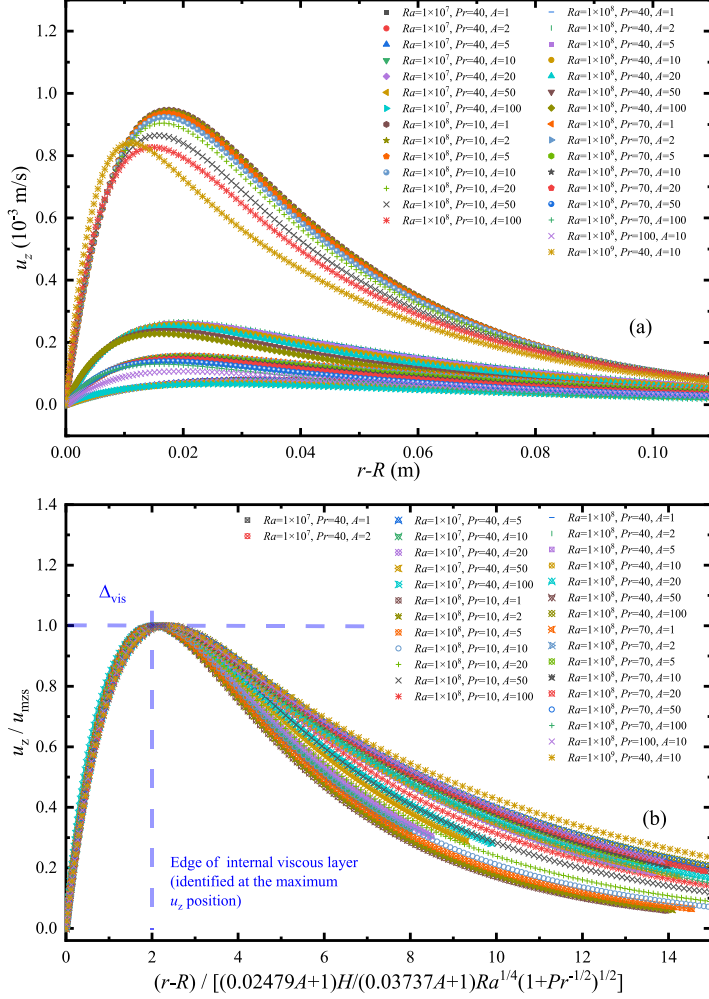
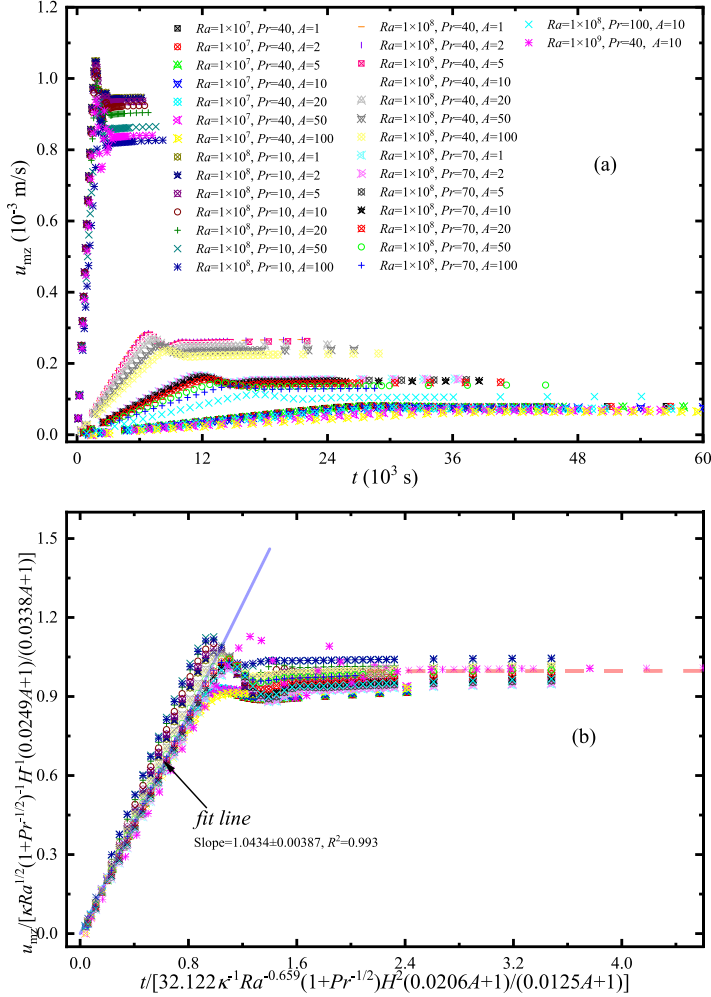


FIG. 13. Velocity profiles adjacent to the heated surface in the steady state: (a) raw data and (b) normalized profile.

Figure 13(a) depicts velocity profiles adjacent to the heated surface at different flow conditions, revealing an initial increase (within the inner viscous layer) followed by a decrease (from  $\Delta_{vis}$  to the outer edge of the viscous layer). The profiles demonstrate that the local velocity does depend on the various flow parameters. Figure 13(b), on the other hand, normalizes the abscissa using Eq. (28) and the ordinate using Eq. (27). Notably, the profiles within the inner viscous layer converge, thus validating the scaling laws described by Eqs. (27) and (28). It is important to note that, compared with the steady-state thermal boundary layer thickness, the steady-state characteristic velocity and inner viscous layer thickness are more influenced by the values of  $A$  and  $Pr$ . This behavior can be explained by the curvature coefficient term, specifically the term  $(1 + mA)/(1 + nA)$ . When the values of  $m$  and  $n$  are close to each other, the effect of  $A$  is insignificant. However, if there is a large difference between  $m$  and  $n$  for the considered flow parameters, the effect of  $A$  becomes significant.

The scaling law of  $u_{mzs}$  could now be determined by the following:

$$u_{mzs} \sim \kappa^2 t Ra^{1.159} H^{-3} (1 + Pr^{-1/2})^{-2} \frac{(1 + 0.0249A)(1 + 0.0125A)}{(1 + 0.0338A)(1 + 0.0206A)}. \quad (30)$$


 FIG. 14. Temporal growth of  $u_{mz}$ : (a) raw data and (b) normalized results.

In this scaling law, the term  $(1 + 0.0249A)(1 + 0.0125A)/(1 + 0.0338A)(1 + 0.0206A)$  represents the curvature effect on  $u_{mz}$ , denoted as  $\Psi'_7(A)$ . Numerical calculations are conducted from  $t = 0$  to  $6t_{sv}$ , with the characteristic velocity  $u_{mz}$  recorded at intervals of  $0.1t_{sv}$ . The resulting velocity time series at different flow conditions are plotted in Fig. 14(a). It is found that the velocity profiles exhibit similarities to the temperature profiles but with a linear correlation between the initial growth of velocity and time. Figure 14(b) normalizes the abscissa using the scaling law of  $t_{sv}$  and the ordinate using Eq. (27). The plot indicates that the profiles approximately sit on the same curve, validating the proposed Eqs. (26) and (27).

To validate the scaling relation given in Eq. (30), the numerically determined  $u_{mz}$  is directly compared with its scaling law at three time instances during the initial growth state, as shown in Fig. 15. The plot demonstrates that Eq. (30) accurately captures the dependencies on Rayleigh number, Prandtl number, curvature, and time. However, it should be noted that there is a slight deviation between the present scaling law and the numerical simulations in some cases of very large  $u_{mz}$ . Nevertheless, with a fitting constant  $R^2 = 0.985$ , it can be concluded that Eq. (30) provides a robust description for the flow of the curved boundary layer.

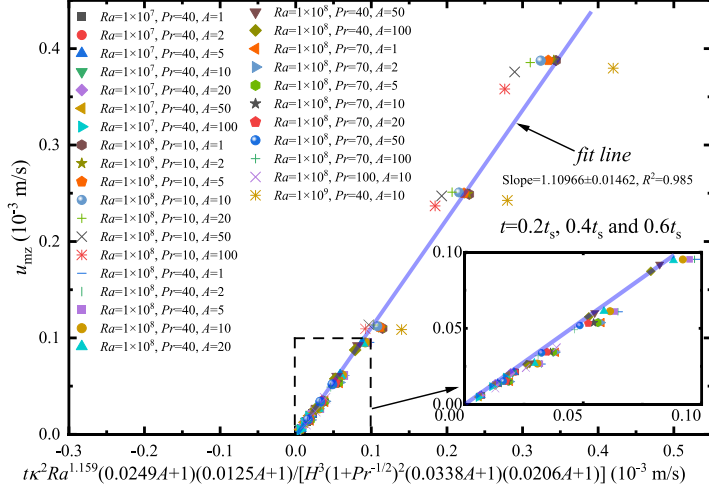


FIG. 15. Numerically obtained early state characteristic velocity  $u_{mz}$  compared against its scaling law  $t\kappa^2 Ra^{1.159}(0.049A + 1)(0.0125A + 1)/[H^3(1 + Pr^{-1/2})^2(0.0338A + 1)(0.0206A + 1)]$  ( $10^{-3}$  m/s).

#### IV. EFFECT OF CURVATURE

The analysis presented above provides important scaling laws that quantify the convective boundary layer flow in an explicit form. These scaling relations can describe a wide range of boundary layer geometries, ranging from flat boundary layers ( $A = 0$ ) to highly curved ones ( $A = 100$ ). The determined scales are summarized in Table II. In comparison with the previous implicit form, these explicit scaling laws offer a much simpler and more straightforward approach for practical applications and calculations. It is crucial to note that the determined scaling laws and  $\Psi'(A)$  are universal, and they are not affected by the choices of dimensional flow parameters.

The effect of curvature on various characterizing variables of the boundary layer flow can be easily demonstrated by plotting the corresponding coefficient  $\Psi'(A)$  of the explicit scaling laws. Figure 16 depicts the values of  $\Psi'_1(A)$  to  $\Psi'_7(A)$  obtained in the previous section. It is important to note that  $\Psi'(A) = 1$  represents the flat-plate flow, where the curvature effect is not present. When  $\Psi'(A) > 1$ , it indicates that the corresponding variable is larger than the value for a flat plate. Conversely, if  $\Psi'(A) < 1$ , it implies that the curved flow parameters are smaller than those of a flat plate. Figure 16 reveals that, due to the presence of curvature, both the characteristic velocity and the boundary layer thickness are reduced compared with the flat-plate problem, with a maximum relative difference of  $\sim -40\%$ . Furthermore, the cutoff time for the initial growth of the boundary layer increases by up to  $\sim 40\%$ . This demonstrates that the curvature effect has a profound influence on the convective boundary layer flow. Authors of previous studies on boundary layer flows have

TABLE II. Explicit scaling laws describing the present curved boundary layer flows.

Initial growth state	Steady state
$\Delta_t \sim \kappa^{1/2} t^{1/2} \frac{(1+0.0125A)^{1/2} (1+0.01118A)}{(1+0.0206A)^{1/2} (1+0.01217A)}$	$\Delta_{ts} \sim H Ra^{-1/4} (1 + Pr^{-1/2})^{1/2} \left( \frac{0.01118A+1}{0.01217A+1} \right)$
$u_{mzs} \sim \kappa^2 t Ra^{1.159} H^{-3} (1 + Pr^{-1/2})^{-2} \frac{(1+0.0249A) (1+0.0125A)}{(1+0.0338A) (1+0.0206A)}$	$u_{mzs} \sim \kappa Ra^{1/2} H^{-1} (1 + Pr^{-1/2})^{-1} \left( \frac{0.0249A+1}{0.0338A+1} \right)$
N/A	$\Delta_{vis} \sim H Ra^{-1/4} (1 + Pr^{-1/2})^{-1/2} \left( \frac{0.02479A+1}{0.03737A+1} \right)$
$t_s \sim \frac{H^2(1+Pr^{-1/2}) (1+0.0206A)}{\kappa Ra^{1/2} (1+0.0125A)}$	
$t_{sv} \sim \frac{H^2(1+Pr^{-1/2}) (1+0.0206A)}{\kappa Ra^{0.659} (1+0.0125A)}$	

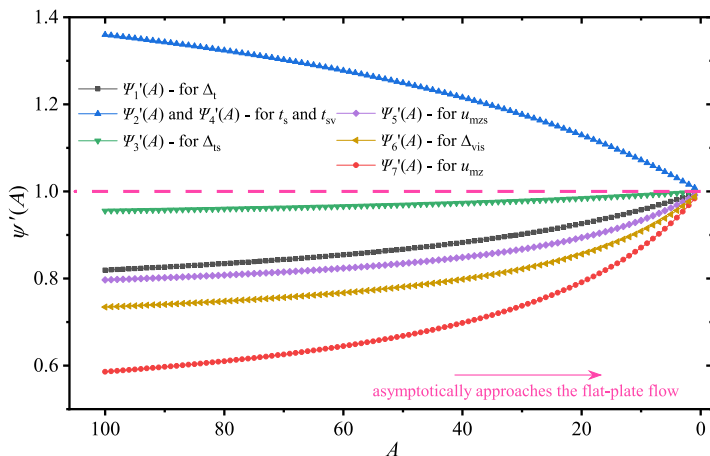


FIG. 16. Effect of curvature on various characterizing parameters of the boundary layer flow.

also shown that the presence of curvature leads to a decrease in the equivalent Rayleigh number of the flow, resulting in a weaker convective boundary layer flow.

## V. CONCLUDING REMARKS

In this paper, we focus on investigating the buoyant boundary layer that develops on the external surface of an isothermally heated vertical cylinder. Numerical calculations reveal that the transient convective flow undergoes three main states: an initial growth, an oscillatory LEE state, and a steady state. These states are similar to those observed in the extensively studied flat plate problems.

In addition to considering the dependencies on the Rayleigh and Prandtl numbers, the influence of the curvature of the heated cylinder, denoted as the parameter  $A$ , is examined and analyzed in particular in this paper. The effect of curvature is accurately described by introducing a dimensionless curvature coefficient  $\Psi'(A)$ . Through numerical regression, important flow variables of the curved boundary layer, such as the thickness and characteristic velocity of the initial and steady states, as well as the durations of the initial growth state, are successfully quantified using the proposed scaling laws. The fitting constants for most of these scaling laws exhibit high values of  $R^2$ ,  $\sim 0.999$ , indicating a strong correlation between the determined scaling relations and the numerical results.

Compared with previous similar studies, the present scaling laws are expressed in an explicit form that provides clearer physical interpretations. These explicit forms make the scaling laws much easier to utilize in practical applications and facilitate a better understanding of the underlying physical phenomena governing the curved boundary layer flow.

## ACKNOWLEDGMENTS

This paper was initiated, conceptualized, and intellectually contributed to by Y.L. C.L. contributed to identifying the dependencies on Prandtl number ( $Pr$ ) and the curvature effect ( $A$ ). After C.L. graduated, Y.Z. took over the project, slightly improved the  $A$  relation, incorporated the  $Ra$  dependency, started over all numerical calculations, and replotted all figures. Y.L. composed the paper, improved all figures, addressed the comments of the reviewer, and supervised the entire research process.

- [1] G. K. Batchelor, Heat transfer by free convection across a closed cavity between vertical boundaries at different temperatures, *Q. Appl. Math.* **12**, 209 (1954).
- [2] A. E. Gill, The boundary-layer regime for convection in a rectangular cavity, *J. Fluid Mech.* **26**, 515 (1966).
- [3] B. Gebhart and R. Mahajan, Characteristic disturbance frequency in vertical natural convection flow, *Int. J. Heat Mass Transfer* **18**, 1143 (1975).
- [4] F. Xu, J. C. Patterson, and C. Lei, Transition to a periodic flow induced by a thin fin on the sidewall of a differentially heated cavity, *Int. J. Heat Mass Transfer* **52**, 620 (2009).
- [5] Y. Liu, C. Lei, and J. C. Patterson, Natural convection in a differentially heated cavity with two horizontal adiabatic fins on the sidewalls, *Int. J. Heat Mass Transfer* **72**, 23 (2014).
- [6] Y. Liu, S. Zhang, H. Huang, Q. Suo, Y. Bian, and Y. Zhao, Enhancing the flow and heat transfer in a convective cavity using symmetrical and adiabatic twin fins, *Int. J. Heat Mass Transfer* **142**, 118447 (2019).
- [7] J. Ke, N. Williamson, S. W. Armfield, S. Norris, and A. Komiya, Law of the wall for a temporally evolving vertical natural convection boundary layer, *J. Fluid Mech.* **902**, A31 (2020).
- [8] N. Ogasawara, J. F. Torres, Y. Kanda, T. Kogawa, and A. Komiya, Resonance-driven heat transfer enhancement in a natural convection boundary layer perturbed by a moderate impinging jet, *Phys. Rev. Fluids* **6**, L061501 (2021).
- [9] Y. Liu and Y. Zhu, Scaling analysis of buoyant boundary layer flow induced by flux heating with a spatial gradient at  $Pr \ll 1$ ,  $Pr \sim 1$  and  $Pr \gg 1$ , *Int. J. Heat Mass Transfer* **204**, 123872 (2023).
- [10] M. Capobianchi and A. Aziz, Laminar natural convection from an isothermal vertical surface to pseudo-plastic and dilatant fluids, *J. Heat Transfer* **134**, 122502 (2012).
- [11] M. Capobianchi and A. Aziz, A scale analysis for natural convective flows over vertical surfaces, *Int. J. Therm. Sci.* **54**, 82 (2012).
- [12] S. Samanta and A. Guha, A similarity theory for natural convection from a horizontal plate for prescribed heat flux or wall temperature, *Int. J. Heat Mass Transfer* **55**, 3857 (2012).
- [13] M. G. Worster and A. M. Leitch, Laminar free convection in confined regions, *J. Fluid Mech.* **156**, 301 (1985).
- [14] X. Chen and F. Hussain, Similarity transformation for equilibrium boundary layers, including effects of blowing and suction, *Phys. Rev. Fluids* **2**, 034605 (2017).
- [15] S. W. Armfield and J. C. Patterson, Wave properties of natural-convection boundary layers, *J. Fluid Mech.* **239**, 195 (1992).
- [16] S. Xin and P. Le Quéré, Linear stability analyses of natural convection flows in a differentially heated square cavity with conducting horizontal walls, *Phys. Fluids* **13**, 2529 (2001).
- [17] H. Jiang, K. Luo, Z. Zhang, J. Wu, and H. Yi, Global linear instability analysis of thermal convective flow using the linearized lattice Boltzmann method, *J. Fluid Mech.* **944**, A31 (2022).
- [18] S. W. Armfield and R. Janssen, A direct boundary-layer stability analysis of steady-state cavity convection flow, *Int. J. Heat Mass Transfer* **17**, 539 (1996).
- [19] T. Abera, S. W. Armfield, M. Behnia, and G. D. McBain, Boundary layer instability of the natural convection flow on a uniformly heated vertical plate, *Int. J. Heat Mass Transfer* **55**, 6097 (2012).
- [20] Y. Liu and S. Ren, Receptivity of incompressible convective boundary layers induced by linear thermal forcing, *Phys. Fluids* **33**, 034127 (2021).
- [21] S. Xin and P. Le Quéré, Direct numerical simulations of two-dimensional chaotic natural convection in a differentially heated cavity of aspect ratio 4, *J. Fluid Mech.* **304**, 87 (1995).
- [22] V. Topalian, T. A. Oliver, R. Ulerich, and R. D. Moser, Temporal slow-growth formulation for direct numerical simulation of compressible wall-bounded flows, *Phys. Rev. Fluids* **2**, 084602 (2017).
- [23] J. C. Patterson and S. W. Armfield, Transient features of natural convection in a cavity, *J. Fluid Mech.* **219**, 469 (1990).
- [24] F. Xu, J. C. Patterson, and C. Lei, Shadowgraph observations of the transition of the thermal boundary layer in a side-heated cavity, *Exp. Fluids* **38**, 770 (2005).
- [25] Y. Zhao, C. Lei, and J. C. Patterson, A PIV measurement of the natural transition of a natural convection boundary layer, *Exp. Fluids* **56**, 9 (2015).

- [26] J. C. Patterson and J. Imberger, Unsteady natural convection in a rectangular cavity, *J. Fluid Mech.* **100**, 65 (1980).
- [27] W. Lin, S. W. Armfield, J. C. Patterson, and C. Lei, Prandtl number scaling of unsteady natural convection boundary layers for  $Pr > 1$  fluids under isothermal heating, *Phys. Rev. E* **79**, 066313 (2009).
- [28] W. Lin, S. W. Armfield, and J. C. Patterson, Cooling of a  $Pr < 1$  fluid in a rectangular container, *J. Fluid Mech.* **574**, 85 (2007).
- [29] F. Xu, J. C. Patterson, and C. Lei, Transient natural convection flows around a thin fin on the sidewall of a differentially heated cavity, *J. Fluid Mech.* **639**, 261 (2009).
- [30] Y. Liu, Scaling of convective boundary layer flow induced by linear thermal forcing at  $Pr < 1$  and  $Pr > 1$ , *Phys. Rev. E* **100**, 043112 (2019).
- [31] Y. Liu, Dynamics and scale analysis of the transient convective flow induced by cooling a  $Pr < 1$  fluid with linear thermal forcing, *Int. J. Heat Mass Transfer* **154**, 119767 (2020).
- [32] Y. Liu and S. Ren, Improved scaling analysis of the transient buoyancy-driven flow induced by a linear temperature gradient, *Int. J. Heat Mass Transfer* **162**, 120386 (2020).
- [33] W. Lin and S. W. Armfield, Natural convection boundary-layer flow on an evenly heated vertical plate with time-varying heating flux in a stratified  $Pr < 1$  fluid, *Numer. Heat Transfer, Part A* **76**, 393 (2019).
- [34] W. Lin, S. Armfield, and M. Khatamifar, Scaling laws for natural convection boundary layer of a  $Pr > 1$  fluid on a vertical solid surface subject to a sinusoidal heating flux in a linearly stratified ambient, *Heat Transfer* **51**, 2956 (2022).
- [35] Y. Liu, Y. Bian, Y. Zhao, S. Zhang, and Q. Suo, Scaling laws for the transient convective flow in a differentially and linearly heated rectangular cavity at  $Pr > 1$ , *Phys. Fluids* **31**, 043601 (2019).
- [36] W. Elenbaas, The dissipation of heat by free convection from vertical and horizontal cylinders, *J. Appl. Phys.* **19**, 1148 (1948).
- [37] R. J. Goldstein and D. Briggs, Transient free convection about vertical plates and circular cylinders, *J. Heat Transfer* **86**, 490 (1964).
- [38] R. P. Dring and B. Gebhart, Transient natural convection from thin vertical cylinders, *J. Heat Transfer* **88**, 246 (1966).
- [39] E. M. Sparrow and L. Lee, Analysis of mixed convection about a horizontal cylinder, *Int. J. Heat Mass Transfer* **19**, 229 (1976).
- [40] S. Xin, P. Le Quéré, and O. Daube, Natural convection in a differentially heated horizontal cylinder: Effects of Prandtl number on flow structure and instability, *Phys. Fluids* **9**, 1014 (1997).
- [41] M. Qiao, Z. Tian, B. Nie, and F. Xu, The route to chaos for plumes from a top-open cylinder heated from underneath, *Phys. Fluids* **30**, 124102 (2018).
- [42] Y. Liu and S. Ren, Scale law analysis of the curved boundary layer evolving around a horizontal cylinder at  $Pr > 1$ , *Phys. Fluids* **33**, 073614 (2021).
- [43] Y. Liu and C. Liu, Unified scale laws for transient convective boundary layers: From flat to curved boundary layers, *Phys. Rev. Fluids* **7**, 054101 (2022).
- [44] Y. Zhao, C. Lei, and J. C. Patterson, Resonance of the thermal boundary layer adjacent to an isothermally heated vertical surface, *J. Fluid Mech.* **724**, 305 (2013).
- [45] J. Merkin, Mixed convection from a horizontal circular cylinder, *Int. J. Heat Mass Transfer* **20**, 73 (1977).
- [46] T. H. Kuehn and R. J. Goldstein, Numerical solution to the Navier-Stokes equations for laminar natural convection about a horizontal isothermal circular cylinder, *Int. J. Heat Mass Transfer* **23**, 971 (1980).
- [47] S. Grossmann and D. Lohse, Thermal Convection for Large Prandtl Numbers, *Phys. Rev. Lett.* **86**, 3316 (2001).
- [48] T. Wei, Scaling of turbulent kinetic energy and dissipation in turbulent wall-bounded flows, *Phys. Rev. Fluids* **5**, 094602 (2020).
- [49] B. Miquel, S. Lepot, V. Bouillaut, and B. Gallet, Convection driven by internal heat sources and sinks: Heat transport beyond the mixing-length or “ultimate” scaling regime, *Phys. Rev. Fluids* **4**, 121501(R) (2019).
- [50] J. C. Patterson, C. Lei, S. W. Armfield, and W. Lin, Scaling of unsteady natural convection boundary layers with a non-instantaneous initiation, *Int. J. Therm. Sci.* **48**, 1843 (2009).

- [51] S. W. Armfield, J. C. Patterson, and W. Lin, Scaling investigation of the natural convection boundary layer on an evenly heated plate, [Int. J. Heat Mass Transfer](#) **50**, 1592 (2007).
- [52] W. Lin and S. W. Armfield, Unified Prandtl number scaling for start-up and fully developed natural-convection boundary layers for both  $Pr \gtrsim 1$  and  $Pr \lesssim 1$  fluids with isothermal heating, [Phys. Rev. E](#) **86**, 066312 (2012).